Synthesis of Multilayer Graphene Balls by Carbon Segregation from Nickel Nanoparticles

Seon-Mi Yoon,[†,△] Won Mook Choi,[‡,△] Hionsuck Baik,[§] Hyeon-Jin Shin,[†] Inyong Song,[⊥] Moon-Seok Kwon,[∥] Jung Jun Bae,[¶] Hansu Kim,[#] Young Hee Lee,[¶] and Jae-Young Choi[†,*]

[†]Graphene Research Center, Samsung Advanced Institute of Technology, Yongin 446-712, Republic of Korea, [‡]School of Chemical Engineering and Bioengineering, University of Ulsan, Ulsan 680-749, Republic of Korea, [§]Analytical Research Division, Korea Basic Science Institute, Seoul 136-713, Republic of Korea, [⊥]Analytical Science Group and [∥]Energy Lab, Samsung Advanced Institute of Technology, Yongin 446-712, Republic of Korea, [¶]BK21 Physics Division, WCU Department of Energy Science, Sungkyunkwan University, Suwon 440-746, Republic of Korea, and [#]Department of Energy Engineering, Hanyang University, Seoul 133-791, Republic of Korea. [△]These authors contributed equally to this work.

ABSTRACT

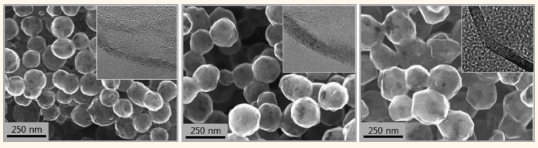

Three-dimensional (3D) structured graphene is a material of great interest due to its diverse applications in electronics, catalytic electrodes, and sensors. However, the preparation of 3D structured graphene is still challenging. Here, we report the fabrication of multilayer graphene balls (GBs) by template-directed carbon segregation using nickel nanoparticles (Ni-NPs) as template materials. To maintain the ball shape of the template Ni-NPs, we used a carburization process using polyol solution as the carbon source and a thermal annealing process to synthesize graphene layers *via* carbon segregation on the outer surface of the Ni-NPs. The resulting GBs were hollow structures composed of multilayer graphene after the removal of core Ni-NPs, and the thickness of the graphene layers and the size of GBs were tunable by controlling the graphene synthesis conditions. X-ray diffraction analysis and *in situ* transmission electron microscope characterization revealed that carbon atoms diffused effectively into the Ni-NPs during the carburization step, and that the diffused carbon atoms in Ni-NPs segregated and successfully formed a graphene layer on the surface of the Ni-NPs during thermal annealing. We also performed further heat treatment at high temperature to improve the quality of the graphene layer, resulting in highly crystalline GBs. The unique hollow GBs synthesized here will be useful as excellent high-rate electrode materials for electrochemical lithium storage devices.

KEYWORDS: graphene · graphene balls · carbon segregation · carburization

Graphene, a single sheet of sp^2-hybridized carbon atoms in a honeycomb lattice, has unique physical and structural properties and has captured the attention of a large number of researchers as a strong candidate for a variety of electronic and energy-related devices and structures. Since mechanical exfoliation of highly ordered pyrolytic graphite for the isolation of graphene sheets was first reported by the Manchester group,[1] many approaches have been developed to synthesize graphene, including sublimation of epitaxial SiC,[2] chemical exfoliation of graphite,[3] and chemical vapor deposition (CVD) using a metal catalyst.[4−6] Among these techniques, the CVD method using a Ni or Cu catalyst is a promising approach for the synthesis of graphene because of its scalability and ease of processing. The Ni-assisted CVD method[7,8] involves bulk carbon diffusion and segregation based on the high solubility of carbon in Ni at high temperatures. In contrast, the Cu-assisted CVD[9,10] method involves a surface catalytic process due to the low solubility of carbon in Cu. Recently, large-area, high-quality graphene sheets have been synthesized using both Ni and Cu catalysts.[11,12]

Three-dimensional (3D) structured graphene is of considerable interest because of its potential applications in sensors, supercapacitors, and catalytic electrodes.[13−15] However, the preparation of 3D structured graphene using both chemical exfoliation and CVD method remains challenging. We developed a simple and scalable method for the synthesis of hollow graphene balls (GBs) *via* template-directed carbon segregation using a Ni nanoparticle (Ni-NP) template. We presented the effective carburization process of Ni-NPs and the carbon segregation to synthesize GBs with controllable graphene thickness and their size and investigated the mechanism of GB synthesis.

RESULTS AND DISCUSSION

GB preparation consists of three steps: (i) carburization process where carbon

* Address correspondence to jaeyoung88.choi@saumsung.com.

Received for review April 8, 2012 and accepted July 5, 2012.

Published online July 05, 2012
10.1021/nn301546z

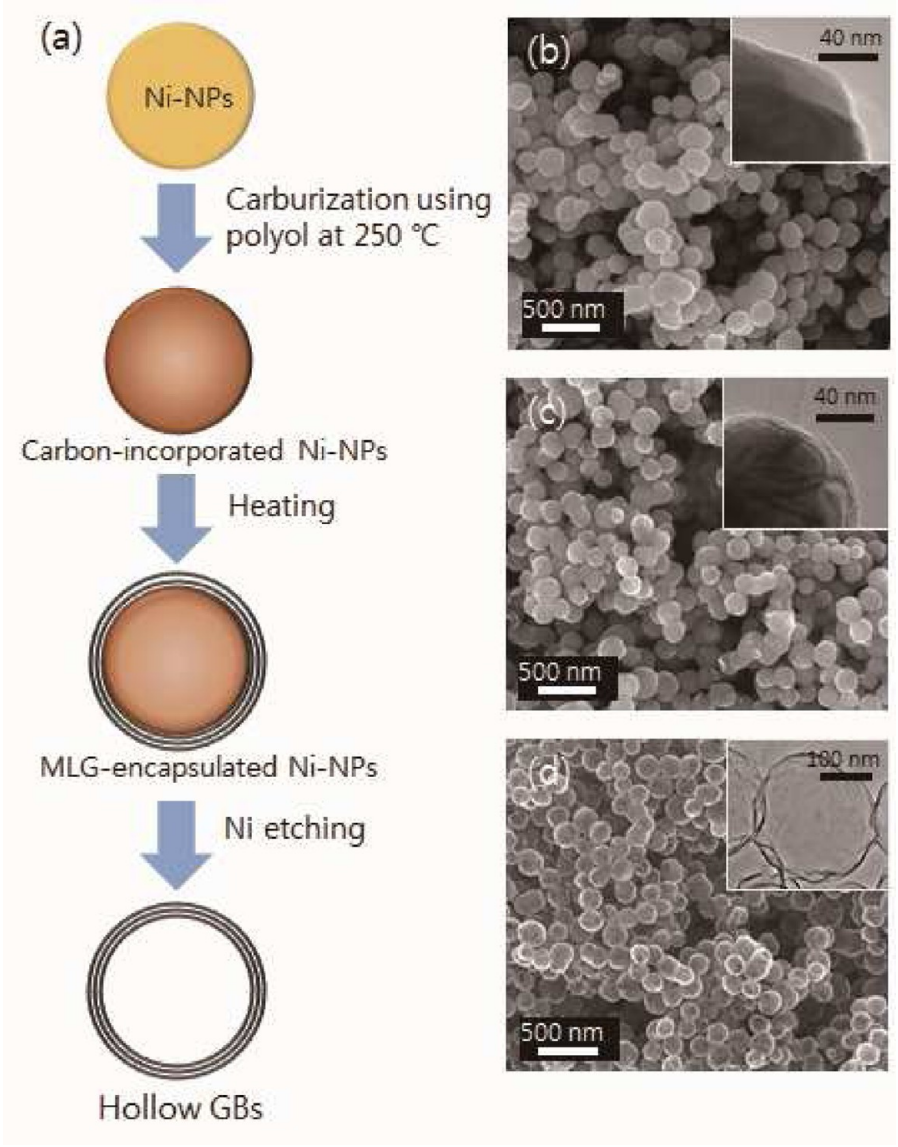

Figure 1. (a) Schematic illustration of the synthesis of hollow GBs. SEM and high-resolution TEM (inset) images of (b) carbon-incorporated Ni-NPs, (c) MLG-encapsulated Ni-NPs, and (d) GBs.

diffused into the starting Ni-NPs using a polyol solution aided by the catalytic reaction of Ni to prepare carbon-incorporated Ni-NPs; (ii) formation of multilayer graphene (MLG)-encapsulated Ni-NPs *via* carbon segregation by thermal annealing of carbon-incorporated Ni-NPs; and (iii) dissolution of the core Ni-NPs using an acidic solution (Figure 1a) to obtain hollow GBs. Starting Ni-NPs with a ball shape and monodisperse size distribution were treated in a polyol solution at 250 °C. Ni effectively decomposes polyol into carbon atoms due to catalytic activation. The decomposed carbon atoms diffuse into the Ni-NPs, resulting in the formation of carbon-incorporated Ni-NPs, the so-called carburization process. As shown in Figure 1b, the carbon-incorporated Ni-NPs retained their original shape and size after the carburization reaction because the carburization reaction was performed at the low temperature of 250 °C to prevent deformation or aggregation of the Ni-NPs, thereby ensuring that the final GBs kept similar shape and size to the starting Ni-NPs. Generally, Ni is carburized by mixing graphite powder with Ni at a high temperature (~1000 °C) in a vacuum for a long period of time (>1 week).[16,17] A high-temperature carburization process cannot be applied to Ni-NPs because fine Ni-NPs would be sintered at these high temperatures, and hence it would be difficult to maintain the shape and size of the initial Ni-NPs. Therefore, in this work, we developed the carburization process at low temperature using a liquid polyol solution to produce carbon-incorporated Ni-NPs that maintained their original shape and size. After the carburization process, the carbon-incorporated Ni-NPs were annealed in an argon atmosphere at 500 °C to synthesize graphene layer on the surfaces of the Ni-NPs. During this annealing process, the carbon atoms diffused by the carburization process were segregated

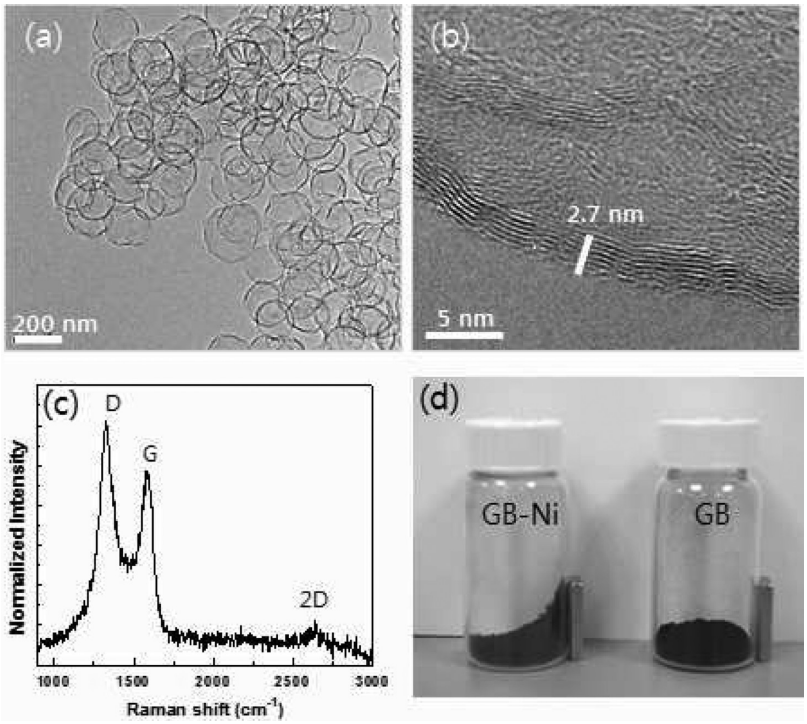

Figure 2. (a) TEM and (b) high-resolution TEM image of GBs. (c) Raman spectrum at a laser excitation wavelength of 633 nm, and (d) photographs of the MLG-encapsulated Ni-NP powder (left) and GB powder (right).

and formed a graphene layer on the surfaces of the Ni-NPs (Figure 1c). Graphitic layer formation on the surface of Ni by high-temperature annealing of carbon-containing Ni is a well-characterized process. Recently, Liu *et al.*[18] reported the synthesis of a graphene layer on the surface of a Ni film using solid carbon segregation instead of using a carbon gas. They prepared catalytic Ni film containing carbon atoms by the deposition of a Ni−carbon compound source, and the graphene layer was synthesized on the Ni surface by annealing at a high temperature (>1000 °C). In this work, we used the relatively low annealing temperature of 500 °C to prevent the Ni-NPs from aggregation. We were therefore able to synthesize MLG-encapsulated Ni-NPs that maintained their original ball shapes without aggregation. Finally, hollow GBs were produced by dissolution of the core Ni-NPs of the prepared MLG-encapsulated Ni-NPs (Figure 1d). Note that the hollow GBs maintained their original ball shape even after the core Ni-NPs were removed with a wet etching process, as shown in the scanning electron microscope (SEM) and transmission electron microscope (TEM) images in Figure 1d.

We used TEM to characterize the structure of the graphene layer in the GBs. Most GBs in Figure 2a are hollow ball structures with the same shape of original Ni-NPs, and the high-resolution TEM image in Figure 2b shows that the typical graphene layer thickness of the GBs was about 2.7 nm, indicating that the GBs comprised approximately eight layers of graphene. Due to high carbon solubility of Ni, mostly multilayer graphene was synthesized on the surface of Ni, and the same behavior occurred in the Ni-assisted CVD method. Moreover, as mentioned above, graphene layers did not collapse or deform during the core Ni-NP etching process. Because of the robust mechanical properties of graphene and the multilayered structures, the GBs maintained their ball shape even after etching out of the core Ni-NPs. In contrast, when only a few layers of graphene were synthesized, the graphene shell collapsed during the core Ni-NP etching process due to a lack of mechanical robustness, resulting in a folded and wrinkled graphene layer (see Supporting Information Figure S1). Raman spectroscopy of the GBs using a 633 nm laser after the removal of the core Ni-NPs revealed three main peaks of graphene. As shown in Figure 2c, D and G peaks appeared in the Raman spectra of the sp^2-carbon material at 1340 and 1580 cm^{-1}, respectively, indicating defects in the graphitic lattice and the graphitic sp^2-structure, and the 2D band around 2650 cm^{-1} is known as a second-order D peak. The prepared GBs had a higher I_D/I_G ratio than CVD-grown graphene at high temperature, showing the defective graphene layer of GBs. To prevent the aggregation of Ni-NPs, we performed the annealing process at 500 °C rather than at ~1000 °C, which is the temperature used to prepare conventional CVD-grown graphene. At this low temperature, the graphene layer was synthesized with the structural defects and amorphous carbon. Furthermore, graphene was synthesized on the spherical surface of the Ni-NPs, resulting in a very small graphene domain, which also contributes to the high I_D/I_G ratio seen in the Raman

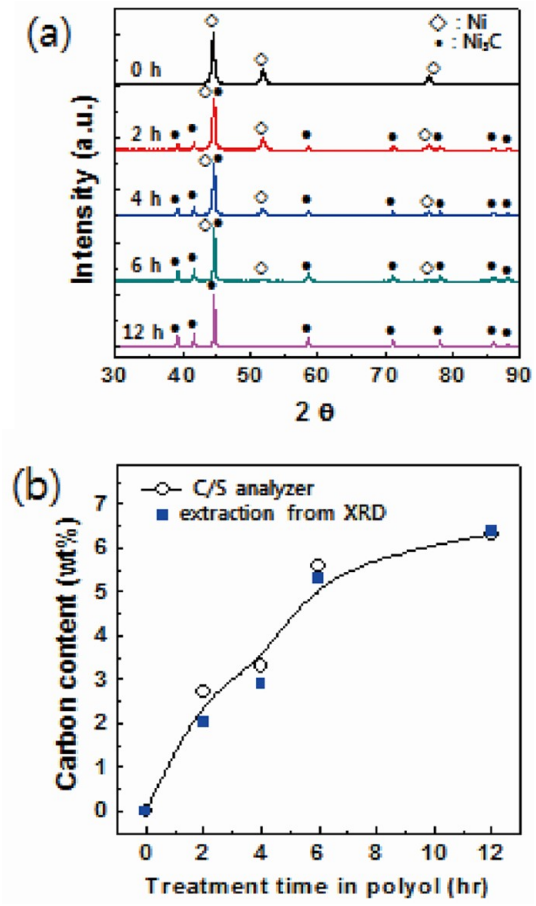

Figure 3. (a) X-ray diffraction patterns of the starting Ni-NPs (top) and the particles obtained after various carburization times in polyol. (b) Carbon content of the carbon-incorporated Ni-NPs as a function of the carburization time.

spectra of the GBs. These results were also attributed to the formation of wavy and discontinuous layered graphene structure, as shown in Figure 2b. Despite the high I_D/I_G ratio, a clear 2D peak was detected in the GBs. These results imply that carburization of a polyol solution and thermal annealing at 500 °C resulted in efficient synthesis of GBs despite the fact that the synthesized graphene layers had defective structures. We took further steps to improve the defective graphene structures, which will be discussed in detail later. The prepared sample powders of MLG-encapsulated Ni-NPs and GBs (the latter obtained after the removal of the core Ni) are shown in Figure 2d. The left image of the MLG-encapsulated Ni-NPs clearly shows that the particles moved toward the wall of the vial in response to a magnetic force exerted by a magnet due to the existence of core Ni, whereas particles in the latter sample (hollow GBs structures without a Ni core) were not attracted to the magnet. Note that our proposed GB synthesis method is simple and scalable to produce a large amount of GBs.

To study the carburization of Ni-NPs using polyol solution, we first characterized the phase changes of Ni-NPs by examining the X-ray diffraction (XRD) patterns of untreated Ni-NPs and carbon-incorporated Ni-NPs after various carburization times at 250 °C, as shown in Figure 3a. The untreated starting Ni-NPs had cubic phase Ni having mainly (111) phase (marked with the open diamond). After 2 h of carburization, a new Ni phase started to appear in the Ni-NPs (marked with filled circles). Examination of the peak position and intensity ratio of the new phase led us to assign the new phase to hexagonal nickel carbide (Ni_3C) (JCPDS 77-0194). As the carburization time increased, the diffraction peak intensity of the cubic phase diminished, while the hexagonal nickel carbide peak intensity increased. After 12 h of carburization, the cubic phase peak finally disappeared, and only the Ni_3C phase was detected, which indicates that the Ni-NPs were converted into nickel carbide nanoparticles by the carburization process in polyol solution. With regard to the carbon content in the carbon-incorporated Ni-NPs, we integrated the diffraction area for each phase from the XRD patterns and also measured the carbon content using a C/S analyzer. As shown in Figure 3b, the carbon content calculated from the XRD data was consistent with the carbon content measured directly using the C/S analyzer; the carbon content increased linearly for the first 6 h of carburization and was saturated at 6.31 wt % of carbon content after 12 h of carburization, at which stage only nickel carbide NPs existed. This saturation value is in good agreement with the stoichiometric carbon content in Ni_3C of 6.39 wt %. These results clearly indicate that the starting Ni-NPs reacted with polyol to effectively induce the cleavage of the C−C bonds of polyol, thereby decomposing it into carbon fragments that diffused into the Ni-NPs, resulting in the formation of the Ni_3C phase during carburization.

Thermal annealing of the carbon-incorporated Ni-NPs is another crucial process for GB formation by the carbon segregation. The Ni_3C phase is known to be unstable at temperatures above 325 °C; at high temperatures, it decomposes into a mixture of phase-separated nickel and graphite phases due to carbon segregation.[19,20] We characterized the carbon segregation behavior of the carbon-incorporated Ni-NPs by *in situ* X-ray diffraction. The XRD patterns at various annealing temperatures after *in situ* thermal annealing of the samples in an X-ray diffractometer under a nitrogen atmosphere are shown in Figure 4a. The heating rate was 10 °C/min, and the holding time was 20 min at each temperature. At 350 °C, the hexagonal Ni_3C phase peaks of the carbon-incorporated Ni-NPs started to decrease and the cubic nickel phase appeared. Above 450 °C, all hexagonal phase peaks disappeared and only cubic nickel phase peaks were observed, as shown in the XRD patterns in Figure 4a. These results were confirmed by the selected area electron diffraction (SAED) patterns (see Supporting Information Figure S3). It reveals that the hexagonal phase of Ni-NPs before the thermal annealing was transformed into the cubic phase after the carbon

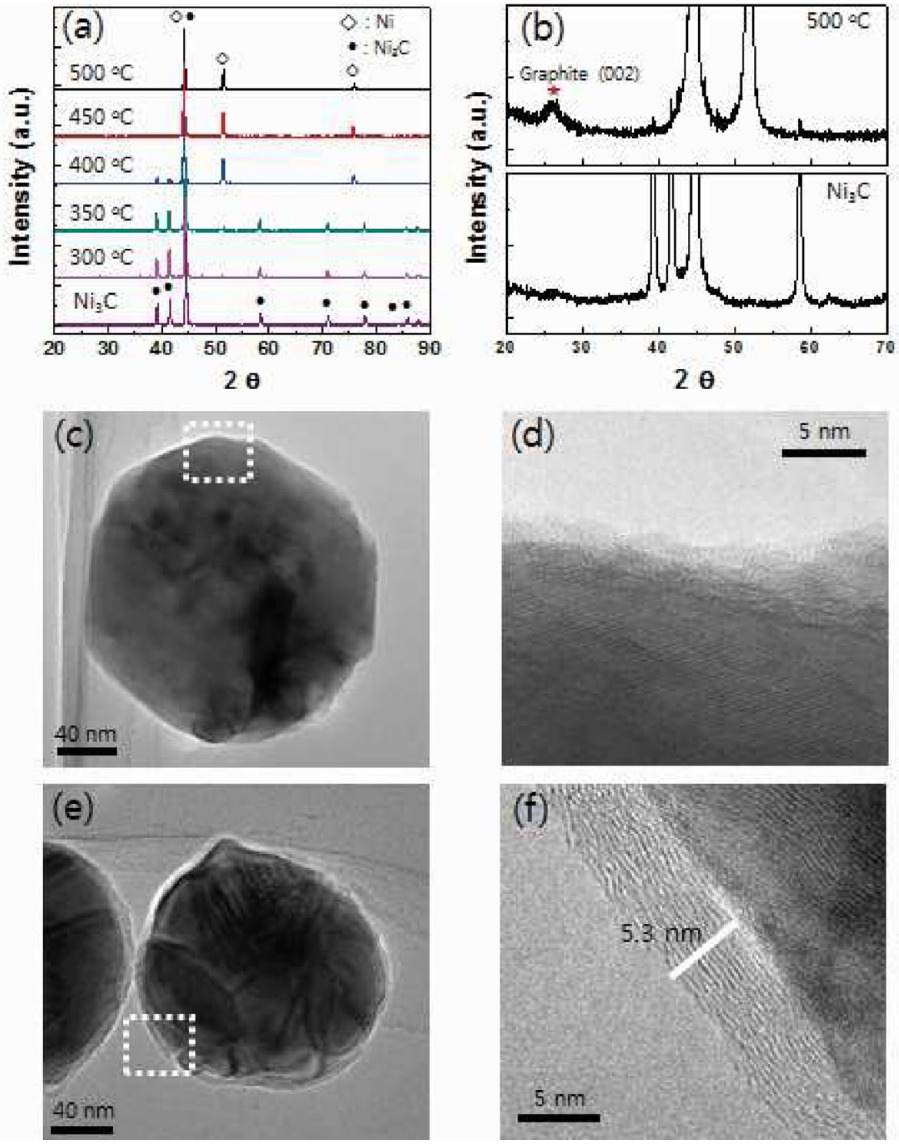

Figure 4. (a) X-ray diffraction patterns of the carbon-incorporated Ni-NPs after *in situ* thermal annealing under a nitrogen atmosphere in an X-ray diffractometer. (b) Synchrotron X-ray diffraction patterns of the starting carbon-incorporated Ni-NPs (bottom) and after *in situ* thermal annealing in an X-ray diffractometer. (c,d) TEM images of the starting carbon-incorporated Ni-NPs, and (e,f) TEM images after *in situ* thermal annealing in an X-ray diffractometer.

segregation by the thermal annealing. More detailed investigations were performed using a synchrotron X-ray source; a trace of a graphite (002) peak at 2θ = 26° clearly appeared after thermal annealing at 500 °C, whereas no graphite peak was found before annealing (Figure 4b). Moreover, high-resolution TEM images showed that graphitic layers formed on the Ni-NPs' surface after thermal annealing (Figure 4e,f); in contrast, no clear graphitic layers were found on the carbon-incorporated Ni-NPs (Figure 4c,d). These results indicate that carbon atoms that diffused into the Ni-NPs during the carburization process segregated and diffused out to form thin graphene layers on the surfaces of the Ni-NPs by the thermal annealing at 500 °C.

To directly observe the formation of graphene layers on the Ni-NP surfaces, we performed *in situ* TEM characterization. Carbon-incorporated Ni-NPs were annealed on a heating stage inside a TEM chamber, and we directly observed graphene layer formation on annealing. *In situ* TEM images of the graphene layers that formed on the surfaces of the Ni-NPs during annealing of the sample are shown in Figure 5. Due to thermal vibration of the particles during *in situ* TEM observations, precise focusing was extremely difficult and we therefore took snapshot micrographs at certain temperature points. Figure 5 confirmed that carbon atoms within the carbon-incorporated Ni-NPs segregated onto the surfaces of the Ni-NPs and successfully formed graphene layers during thermal annealing, and TEM images clearly showed that the number of graphene layers increased in proportion to the annealing temperature. Graphene layers did not form initially

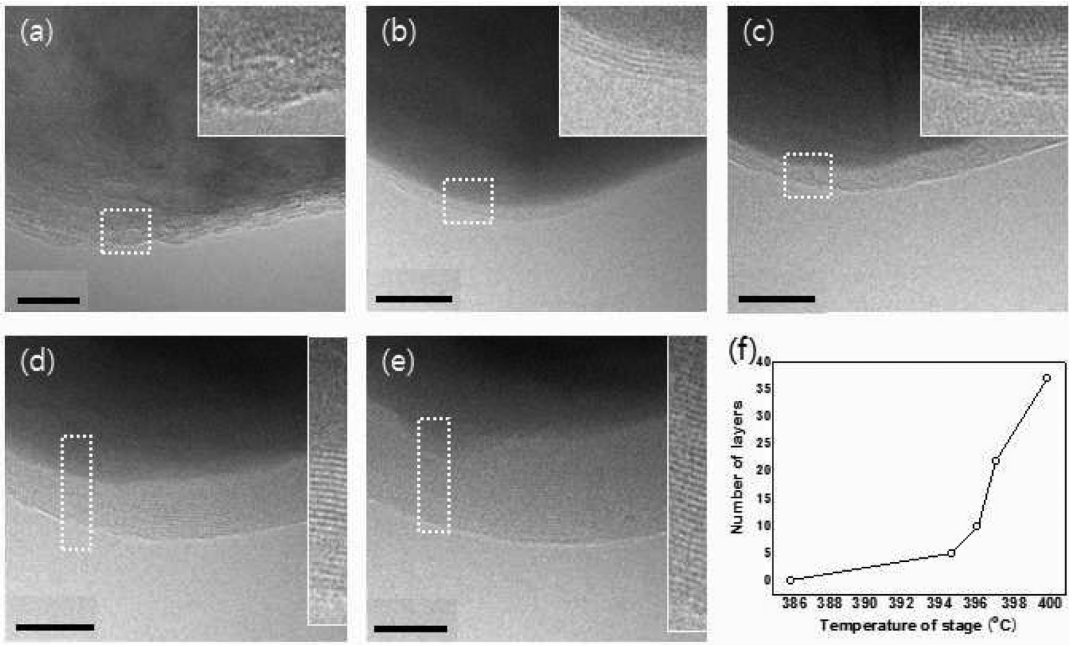

Figure 5. *In situ* **TEM characterization of the formation of graphene layers upon heating the carbon-incorporated Ni-NPs, (a) 386 °C, (b) 395 °C, (c) 396 °C, (d) °397 C, (e) 400 °C, and corresponding high-resolution TEM images (insets). (f) Number of graphene layers grown at various heating temperature. The scale bar represents 10 nm.**

around 380 °C but increased rapidly above 395 °C (Figure 5f). Moreover, we demonstrated that the number of graphene layers can be controlled by controlling the annealing time at a given annealing temperature (see Supporting Information Figure S2a−c); the thickness of the graphene layers increased as the annealing time at 500 °C increased. These results confirms that, for a given carbon content of the Ni-NPs, the amount of carbon atoms that reach the surface of the Ni-NPs was determined by the diffusion length, which is limited by the diffusion time. Various sizes of GBs were also obtained by synthesizing GBs using starting Ni-NPs with various diameters (see Supporting Information Figure S2d−f); the diameter of GBs increased as the diameter of starting Ni-NPs increased.

As shown in Figure 2c, the crystallinity of the as-prepared GBs was still low, considering the high I_D/I_G ratio in the Raman spectra and the defective layered structure in the TEM images. There were amorphous carbons and structural defects in the graphene crystal such as pentagons, heptagons, and vacancies due mainly to our use of a thermal annealing temperature of 500 °C. It is well-known that, for metal-assisted CVD graphene growth, a low I_D/I_G ratio is generally observed for graphene grown at temperatures >900 °C. To remove the defects and enhance the crystallinity of the GBs, we performed the heat treatment with the hollow GBs at 900 and 1200 °C. Figure 6a shows GBs after the heat treatment at 900 °C for 1 h. The heat-treated GBs maintained their spherical ball shape without deformation and aggregation. The detailed observation of their graphene layers by TEM (Figure 6b) indicated that the graphene layers became flat and continuous structures compared to the as-prepared GBs in Figure 2b, which had a somewhat wavy and discontinuous layered structure. The heat treatment of GBs at 1200 °C yielded GBs with some interesting characteristics. SEM and TEM images of the GBs are shown in Figure 6c,d after the heat treatment at 1200 °C. The morphology of the GBs changed from spherical to polyhedral, and some of them aggregated due to interdiffusion during heat treatment. High-resolution TEM images of the wall structure also revealed that the round morphology of the GBs was transformed into a faceted morphology due to significantly flat layered structural development. We attribute these thermally induced morphological transformations of the GB structures to density changes in the GBs induced by an increase of crystallinity and crystalline size, which creates strain in the confined GBs' structures and subsequently yields a straight layer of graphene with a bent structure. This result is consistent with that of a previous study[21] that investigated the effects of heating multiwalled carbon nanotubes (MWCNTs) at high temperatures. The authors of that study reported a change in morphology from wavy layers into straight layers after high-temperature treatment. These structural effects of the heat treatment of GBs are in good agreement with the results of XRD and Raman analyses. The XRD and Raman spectra of the samples heat-treated at 900 and 1200 °C are shown in Figure 6e,f. The (002) peaks of graphite detected in the XRD data were much sharper than that of the as-prepared GBs in Figure 4b, indicating the improvement of the layered

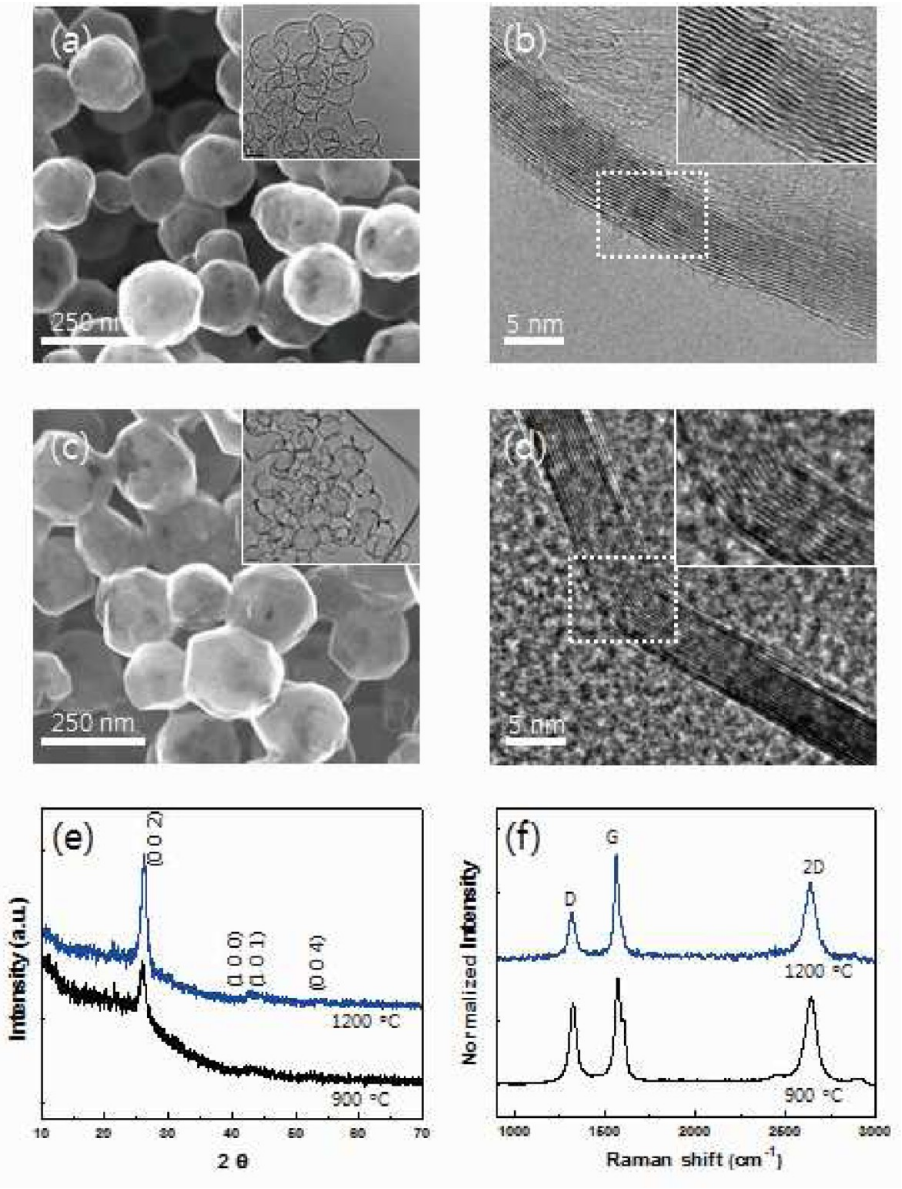

Figure 6. SEM and TEM images of GBs heat-treated (a,b) at 900 °C for 1 h and (c,d) at 1200 °C for 1 h. (e) X-ray diffraction patterns and (f) Raman spectra of the GBs heat-treated at 900 and 1200 °C.

structures of graphene. To determine the peak sharpness quantitatively, we calculated full width at half-maximum (fwhm) values from (002) peaks of graphite in the XRD data shown in Figure 6e. As-prepared GBs had a fwhm value of 1.86, whereas the GBs heat-treated at 900 and 1200 °C had a fwhm value of 1.12 and 0.95, respectively, suggesting that the crystallinity and flat layer stack of the GBs was improved by heat treatment. We confirmed these results by investigating the Raman spectra, which revealed clearly the decrease of the D peak with the increase of the 2D peak. The I_D/I_G ratio of GBs heat-treated at 1200 and 900 °C was 0.447 and 0.770, respectively, indicating that the defects in the GBs were removed and recrystallized with larger crystalline size of graphene after heat treatment at high temperature. Moreover, the 2D peak at about 2650 cm^{-1} in Figure 6f, another indicator of the crystallinity of graphene, was more prominent in the heat-treated GBs than the as-prepared GBs. These results clearly indicate that thermal treatment of GBs effectively increases their crystallinity and crystalline size and is accompanied by a transition in morphology from spherical to polyhedral.

As proof-of-concept of one potential application of the GBs, we evaluated the electrochemical performance of the as-prepared GBs and heat-treated GBs (1200 °C) as anodes for lithium-ion batteries. The cycle performance of the as-prepared and heat-treated GBs at various current density conditions is shown in Figure 7. Both types of GBs showed a certain capacity fading as the cycle number and current density rate increased, which we attributed to the formation of a

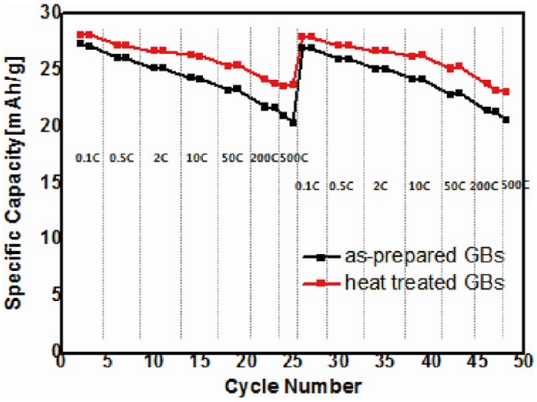

Figure 7. Cycle performances of the as-prepared GBs and the heat-treated GBs. The current density (*C*) was 300 mA/g.

solid electrolyte interface (SEI) film on the electrode surface of the GBs due to electrolyte decomposition and the formation of lithium organic compounds. Even at an extremely high current density rate, the heat-treated and as-prepared GBs exhibited excellent capacity retention values of 82.3 and 75.5%, respectively, which could be due to their unique structure, that is, a hollow ball shape with thin graphene layers (about 3 nm). These results indicate that GBs are excellent high-rate electrode materials for electrochemical lithium storage devices. It should also be noted that even after the high current density rate measurements, the specific capacity at each current rate recovered almost to the initial value of 97.5% for the heat-treated GBs and to 94.9% for the as-prepared GBs. These low-capacity GB anodes still have some disadvantages compared with commercial lithium-ion batteries and are not competitive with conventional carbon anodes; however, their excellent high-rate cycle performance with high electrochemical reversibility makes these GBs suitable for electrochemical applications. Moreover, the low specific capacity of the GBs could be improved by modifying the structures of GBs for high surface area and creating the composite electrodes with high-capacity electrode materials such as Si or Sn.

CONCLUSIONS

We developed a template-directed method to synthesize hollow GBs using Ni-NPs as a template. We performed a carburization process to facilitate carbon diffusion into Ni-NPs using a polyol solution and thermal annealing to stimulate carbon segregation, resulting in graphene layer formation on the surfaces of Ni-NPs. The prepared GBs maintained their spherical ball shape and did not aggregate during the thermal annealing process and even after removal of the core Ni-NPs, yielding hollow GBs composed of multilayer graphene. The detailed investigation using XRD and *in situ* TEM characterization revealed that the carburization of Ni-NPs with polyol solution and the carbon segregation by thermal annealing are reliable approaches for graphene synthesis on the surfaces of the Ni-NPs. We also obtained high-quality GBs by further heat treatment at high temperatures. The unique hollow structures of GBs make them suitable for application in future electronic devices, energy electrode materials for lithium-ion batteries and supercapacitors, and as catalysts. Moreover, the template-directed GB synthesis approach proposed in this work is a versatile and scalable technique that can be used to fabricate structured graphene materials.

METHODS

Preparation of GBs. Ni-NPs were prepared by reducing nickel chloride in aqueous solution. The prepared Ni-NPs were transferred into polyol solution, which is a triethylene glycol (TEG) solution that contains a small amount of NaOH aqueous solution. Keeping the system at a temperature of 250 °C for an appropriate time finally led to the formation of carbon-incorporated Ni-NPs. The prepared samples were placed in a furnace and annealed in an argon atmosphere at 500 °C, resulting in MLG-encapsulated Ni-NPs. The hollow GBs were obtained by dissolving the core Ni-NPs in a dilute hydrochloric acid solution for 12 h.

Electrochemical Measurements. The electrodes were prepared by spreading slurries of 40 wt % GBs and 60 wt % polyvinylidene fluoride (Solvay Solexis, SOLEF 6020) dissolved in *N*-methyl-2-pyrrolidone onto 15 μm thick copper foil current collectors. After heating at 80 °C for 2 h and pressing by a roll press machine, circular electrodes (12 mm diameter) with a typical loading of 1.5 mg/cm^2 GC were dried at 120 °C for 2 h in a vacuum oven. Then, 2032 coin-type cells were used in charge–discharge measurements to study the electrochemical properties of the GBs. Each coin cell consisted of a working electrode, a polyolefin separator (Celgard), and a lithium-foil (FMC Corporations, USA) counter electrode. The electrolyte was 1.3 M $LiPF_6$/ethylene carbonate diethyl carbonate (EC-DEC, 3:7, v/v, Panax etec, Korea). The tests were conducted with steps of constant-current/constant-voltage (CC/CV) charging (at 0.22 mA/cm^2, 0.01 V charging voltage) and CC discharging (at various rates, end-of-discharge voltage of 2.0 V) using TOSCAT-5200 (TOYO, Japan).

Material Characterizations. The shape, size, and surface morphology of the starting Ni-NPs, graphene-encapsulated Ni-NPs, and GBs were investigated using a field-emission scanning electron microscope (SEM; Hitachi S-4700). The thickness and structure of the graphene layers were observed using a TEM (FEI Titan F30). The structure of the graphene layers was also characterized by micro-Raman spectroscopy (Renishaw RM1000-Invia). An excitation energy of 1.96 eV (632.8 nm, He–Ne laser) with a Rayleigh line rejection filter, which accepts a spectral range of 50–3200 cm^{-1}, was used in this study. Structural evolution of the carbon-incorporated Ni-NPs during high-temperature annealing was verified by using a TEM equipped with an *in situ* heating instrument and was performed using a JEOL atomic resolution microscope accelerated by 1 MeV at KBSI (Korea Basic Science Institute). Samples were heated up to 350 °C at a rate of 20 °C/min and then 1 °C/min from 350 to 400 °C. Carbon content in the carbon-incorporated Ni-NPs was measured with a C/S analyzer (Horiba). Phase changes of the Ni-NPs during polyol treatment and high-temperature annealing were identified using various X-ray diffractometers, an XRD (Philips, X'pert) with Cu Kα radiation (λ = 1.5418 Å), an XRD (Rigagu) equipped with an *in situ* heating instrument and a high-resolution synchrotron powder XRD on the 8C2 line at Pohang Light Sources, Korea.

Conflict of Interest: The authors declare no competing financial interest.

Acknowledgment. W.M.C. acknowledges financial support by Basic Science Research Program through the National Research Foundation of Korea (NRF) funded by the Ministry of Education, Science and Technology (2012R1A1A1015124).

Supporting Information Available: Further detail data for the collapsed GBs, the GBs prepared with various graphene layer thicknesses, SAED data of Ni-NPs, thickness variation of the graphene layer, and the charge–discharge profiles of the as-prepared and the heat-treated GBs. This material is available free of charge *via* the Internet at http://pubs.acs.org.

REFERENCES AND NOTES

1. Novoselov, K. S.; Geim, A. K.; Morozov, S. V.; Jiang, D.; Zhang, Y.; Dubonos, S. V.; Grigorieva, I. V.; Firsov, A. A. Electric Field Effect in Atomically Thin Carbon Films. *Science* **2004**, *306*, 666–669.
2. Emtsev, K. V.; Bostwick, A.; Horn, K.; Jobst, J.; Kellogg, G. L.; Ley, L.; McChesney, J. L.; Ohta, T.; Reshanov, S. A.; Rohrl, J. Towards Wafer-Size Graphene Layers by Atmospheric Pressure. *Nat. Mater.* **2009**, *8*, 203–207.
3. Eda, G.; Fanchini, G.; Chhowalla, M. Large-Area Ultrathin Films of Reduced Graphene Oxide as a Transparent and Flexible Electronic Material. *Nat. Nanotechnol.* **2008**, *3*, 270–274.
4. Reina, A.; Jia, X.; Ho, J.; Nezich, D.; Son, H.; Bulovic, V.; Dresselhaus, M. S.; Kong, J. Large Area, Few-Layer Graphene Films on Arbitrary Substrates by Chemical Vapor Deposition. *Nano Lett.* **2009**, *9*, 30–35.
5. Kim, K. S.; Zhao, Y.; Jang, H.; Lee, S. Y.; Kim, J. M.; Kim, K. S.; Ahn, J. H.; Kim, P.; Choi, J. Y.; Hong, B. H. Large-Scale Pattern Growth of Graphene Films for Stretchable Transparent Electrodes. *Nature* **2009**, *457*, 706–710.
6. Li, X.; Cai, W.; An, J.; Kim, S.; Nah, J.; Yang, D.; Piner, R.; Velamakanni, A.; Jung, I.; Tutuc, E.; *et al.* Large-Area Synthesis of High-Quality and Uniform Graphene Films on Copper Foils. *Science* **2009**, *324*, 1312–1314.
7. Yu, Q.; Lian, J.; Siriponglert, S.; Li, H.; Chen, Y. P.; Pei, S. S. Graphene Segregated on Ni Surfaces and Transferred to Insulators. *Appl. Phys. Lett.* **2008**, *93*, 113103.
8. Chae, S. J.; Gunes, F.; Kim, K. K.; Kim, E. S.; Han, G. H.; Kim, S. M.; Shin, H. J.; Yoon, S. M.; Choi, J. Y.; Park, M. H.; *et al.* Synthesis of Large-Area Graphene Layers on Poly-Nickel Substrate by Chemical Vapor Deposition: Wrinkle Formation. *Adv. Mater.* **2009**, *21*, 2328–2323.
9. Wofford, J. M.; Nie, S.; McCarty, K. F.; Bartelt, N. C.; Dubon, O. D. Graphene Islands on Cu Foils: The Interplay between Shape, Orientation, and Defects. *Nano Lett.* **2010**, *10*, 4890–4896.
10. Wood, J. D.; Schmucker, S. W.; Lyons, A. S.; Pop, E.; Lyding, J. W. Effects of Polycrystalline Cu Substrate on Graphene Growth by Chemical Vapor Deposition. *Nano Lett.* **2011**, *11*, 4547–4554.
11. Lee, Y.; Bae, S.; Jang, H.; Jang, S.; Zhu, S.-E.; Sim, S. H.; Song, Y. I.; Hong, B. H.; Ahn, J.-H. Wafer-Scale Synthesis and Transfer of Graphene Films. *Nano Lett.* **2010**, *10*, 490–493.
12. Bae, S.; Kim, H.; Lee, Y.; Xu, X.; Park, J.-S.; Zheng, Y.; Balakrishnan, J.; Lei, T.; Kim, H. R.; Song, Y. I.; *et al.* Roll-to-Roll Production of 30-Inch Graphene Films for Transparent Electrodes. *Nat. Nanotechnol.* **2010**, *5*, 574–578.
13. Chen, Z.; Ren, W.; Gao, L.; Liu, B.; Pei, S.; Cheng, H.-M. Three-Dimensional Flexible and Conductive Interconnected Graphene Networks Grown by Chemical Vapour Deposition. *Nat. Mater.* **2011**, *10*, 424–428.
14. Chen, W.; Yan, L. *In Situ* Self-Assembly of Mild Chemical Reduction Graphene for Three-Dimensional Architectures. *Nanoscale* **2011**, *3*, 3132–3137.
15. Bi, H.; Huang, F.; Liang, J.; Tang, Y.; Lü, X.; Xie, X.; Jiang, M. Large-Scale Preparation of Highly Conductive Three Dimensional Graphene and Its Applications in CdTe Solar Cells. *J. Mater. Chem.* **2011**, *21*, 17366–17370.
16. Eizenberg, M.; Blakely, J. M. Carbon Monolayer Phase Condensation on Ni(111). *Surf. Sci.* **1979**, *82*, 228–236.
17. Yamazaki, S.; Tanaka, M.; Tanaka, S.; Fuginami, M.; Uemori, R.; Fujita, D.; Homma, T.; Ono, M. Atomic Images and Defect Structures of the Epitaxially Precipitated Carbon Layers on Ni(111) Surface. *J. Vac. Sci. Technol., B* **1991**, *9*, 883–885.
18. Liu, N.; Fu, L.; Dai, B. Y.; Yan, K.; Liu, X.; Zhao, R. Q.; Zhang, Y. F.; Liu, Z. F. Universal Segregation Growth Approach to Wafer-Size Graphene from Non-noble Metals. *Nano Lett.* **2011**, *11*, 297–303.
19. Joyce, E. L., Jr.; Jervis, T. R. Observations of Grain Growth and Metastable Phase Decomposition in Nanocrystalline Materials. *Scr. Mater.* **1988**, *22*, 1313–1316.
20. Sinharoy, S.; Levenson, L. L. The Formation and Decomposition of Nickel Carbide in Evaporated Nickel Films on Graphite. *Thin Solid Films* **1978**, *53*, 31–36.
21. Kim, Y. A.; Hayashi, T.; Endo, M.; Kaburagi, Y.; Tsukada, T.; Shan, J.; Osato, K.; Tsuruoka, S. Synthesis and Structural Characterization of Thin Multi-Walled Carbon Nanotubes with a Partially Facetted Cross Section by a Floating Reactant Method. *Carbon* **2005**, *43*, 2243–2250.